Atmos. Meas. Tech. Discuss., 8, 10249–10282, 2015
www.atmos-meas-tech-discuss.net/8/10249/2015/
doi:10.5194/amtd-8-10249-2015

Atmospheric Measurement Techniques Discussions
Open Access

This discussion paper is/has been under review for the journal Atmospheric Measurement Techniques (AMT). Please refer to the corresponding final paper in AMT if available.

Calibration methods for rotating shadowband irradiometers and evaluation of calibration duration

W. Jessen[1,2], S. Wilbert[1], B. Nouri[1], N. Geuder[3], and H. Fritz[2]

[1]German Aerospace Center (Deutsches Zentrum für Luft- und Raumfahrt e.V.), Institute of Solar Research, Qualification/Solar Energy Meteorology, Plataforma Solar de Almería, Carretera de Senés s/n, km 5, 04200 Tabernas, Spain
[2]Department VIII, Mechanical Engineering, Event Technology, Process Engineering, Beuth University of Applied Sciences Berlin (Beuth Hochschule für Technik Berlin), Luxemburger Straße 10, 13353 Berlin, Germany
[3]Faculty of Civil Engineering, Building Physics and Business Management, University of Applied Sciences Stuttgart (Hochschule für Technik Stuttgart), Schellingstraße 24, 70174 Stuttgart, Germany

Received: 25 June 2015 – Accepted: 16 September 2015 – Published: 6 October 2015

Correspondence to: S. Wilbert (stefan.wilbert@dlr.de)

Published by Copernicus Publications on behalf of the European Geosciences Union.

Abstract

Resource assessment for Concentrated Solar Power (CSP) needs accurate Direct Normal Irradiance (DNI) measurements. An option for such measurement campaigns are Rotating Shadowband Irradiometers (RSIs) with a thorough calibration. Calibration of RSIs and Si-sensors in general is complex because of the inhomogeneous spectral response of such sensors and incorporates the use of several correction functions. A calibration for a given atmospheric condition and air mass might not work well for a different condition. This paper covers procedures and requirements for two calibration methods for the calibration of Rotating Shadowband Irradiometers. The necessary duration of acquisition of test measurements is examined in regard to the site specific conditions at Plataforma Solar de Almeria (PSA) in Spain. Data sets of several long-term calibration periods from PSA are used to evaluate the deviation of results from calibrations with varying duration from the long-term result. The findings show that seasonal changes of environmental conditions are causing small but noticeable fluctuation of calibration results. Certain periods (i.e. November to January and April to May) show a higher likelihood of particularly adverse calibration results. These effects can partially be compensated by increasing the inclusions of measurements from outside these periods.

Consequently, the duration of calibrations at PSA can now be selected depending on the time of the year in which measurements are commenced.

1 Introduction

Concentrated Solar Power (CSP) projects require accurate assessment of the available direct beam resource. Ground measurements have to be combined with satellite derived data for this assessment. These ground measurements can be obtained with solar trackers and pyrheliometers or with Rotating Shadowband Irradiometers (RSIs). Due to its lower susceptibility to soiling RSIs have an important advantage over ther-

AMTD

8, 10249–10282, 2015

mopile pyrheliometers during long-term deployment at remote and inaccessible sites where daily cleaning of the instrument's aperture is not possible (Geuder and Quaschning, 2006; Pape et al., 2009; Maxwell et al., 1999). Further advantages of RSIs compared to pyrheliometer stations are the installation and maintenance costs and the typically achieved data availability.

RSIs consist of a pyranometer and a shadowband that rotates e.g. once per minute around the pyranometer such that the sensor is shaded for some time. Examples for RSIs can be seen in Fig. 1. When the shadowband is in its rest position, the global horizontal irradiance (GHI) is measured. Diffuse horizontal irradiance (DHI) is measured during the rotation and direct normal irradiance (DNI) is calculated using GHI, DHI and the solar zenith angle. RSIs are often called RSRs or RSP, depending on the instrument manufacturer. Instead of irradiometer, radiometer or pyranometer appear in these names. The notation RSI refers to all instruments measuring irradiance by use of a rotating shadowband. Two types of RSIs can be distinguished: RSIs with continuous and discontinuous rotation. The operational principal of RSIs with continuous rotation is explained in the following. At the beginning of the rotation, the shadowband is below the pyranometer, in its rest position. The rotation is performed with constant angular velocity and takes approximately 1 to 2 s. During the rotation the irradiance is measured with a high and constant sampling rate (e.g. 1 kHz). This measurement is analysed in order to derive GHI and DHI for the time of the rotation. In this work only RSIs with continuous rotation of the shadowband are discussed. Such RSIs need a pyranometer with a fast response time ($\ll 1$ ms, e.g. 10 µs). Thus, thermal sensors as described in ISO 9060 cannot be applied. Instead, semiconductor sensors are used, e.g. the Si-pyranometer LI-200SA (LI-COR, 2004).

RSIs with discontinuous rotation do not use a continuous and fast rotation, but a discontinuous step wise rotation. Instead of measuring the complete signal during the rotation, only four points of it are measured (Harrison et al., 1994). First, the GHI is measured while the shadowband is in the rest position. Then the shadowband rotates from the rest position towards the position where it nearly shades the pyranometer,

AMTD
8, 10249–10282, 2015

stops and a measurement is taken (e.g. during 1 s). Then it continues the rotation towards the position in which the shadow lies centered on the pyranometer and another measurement is taken. The last point is measured in a position in which the shadow just passed the pyranometer. Such RSIs require a much more accurate adjustment of the instrument's azimuth orientation than RSIs with continuous rotation as well as an exact time adjustment and are not discussed here.

So far, RSIs with continuous rotation use the LI-COR LI-200SA pyranometer. This photodiode instrument underlies systematic errors caused by cosine and temperature effects and its non-uniform spectral responsivity. A number of correction functions can be employed to reduce these errors significantly. The combination of the publications King and Myers (1997), King et al. (1998), Augustyn et al. (2004) and Vignola (2006) provide a set of functions which use the ambient temperature, solar zenith angle, air mass, GHI and DHI as input parameters. Geuder et al. (2008) introduced a separate set of correction functions which uses an additional spectral parameter determined from GHI, DHI, and DNI. An improved version of these corrections has been analysed in Geuder et al. (2010).

A thorough calibration of RSIs with application of the correction functions is required for utmost quality of measurements. The calibration procedures of thermopile pyranometers and pyrheliometers are well documented in standards such as ISO 9059, ISO 9846 and ISO 9847. These standards are not directly applicable to RSIs due to their inherent characteristics, especially because of the spectral selectivity of the Si-pyranometers used in RSIs. The inhomogeneous spectral response results in the problem that a calibration for a given atmospheric condition and air mass might not work well for a different condition with a corresponding different spectrum. Hence, specific calibration procedures for RSIs were developed e.g. by the German Aerospace Center (DLR). DLR's calibration methods include significantly longer measuring periods and require measurements from a wider range of meteorological conditions than the before mentioned standards. The longer calibration durations avoid that the calibration is derived from single extreme spectral conditions. In further deviation from

AMTD
8, 10249–10282, 2015

the ISO standards for thermopile sensors the RSI calibration methods by DLR assign more than one calibration factor for each instrument since multiple components of solar irradiance with differing spectral composition and sensor responsivity are determined.

These RSI calibration methods have been applied at the Plataforma Solar de Almeria (PSA) for a number of years. However, some details are still under investigation to increase the reliability. A thorough assessment of the necessary calibration duration and seasonal influences on calibration results has now been carried out with several years of measurements from five RSIs. This paper outlines two RSI calibration procedures developed by DLR and presents the site specific findings in regard to calibration duration and seasonal influences at PSA.

2 Investigated RSI calibration methods

This paper discusses two calibration methods applied at PSA. Each of both calibration methods corresponds to a different set of correction functions. Therefore, the following differentiates between the calibration method corresponding to functional corrections by Geuder et al. (2008) (called DLR2008) and the calibration method corresponding to functional corrections by King, Myers, Augustyn and Vignola as published in King and Myers (1997), King et al. (1998), Augustyn et al. (2004), and Vignola (2006) (called VigKing). Some functions in the latter set have been published in varying versions. The working set used in VigKing calibrations therefore was summarized in Wilbert et al. (2015).

Both methods assign individual calibration factors to different irradiance components in addition to the LI-200SA Silicon-Pyranometer manufacturer's (LI-COR) calibration factor. The RSI is compared to a reference direct normal irradiance (DNI_{Ref}) and a reference diffuse horizontal irradiance (DHI_{Ref}) that are measured with a ISO 9060 first class pyrheliometer and a secondary standard pyranometer shaded with a shadowball, respectively. More specifically, Kipp&Zonen CH1 or CHP1 pyrheliometers and CMP21 or CMP11 are used depending on the time interval under evaluation. The ref-

AMTD
8, 10249–10282, 2015

erence global horizontal irradiance (GHI_{Ref}) is calculated from both reference instruments since this yields higher accuracy than GHI measurement by a pyranometer (see ISO 9060). Nonetheless, a second pyranometer that measures GHI directly is used to control the reference measurements by redundancy check.

Data collection at PSA (latitude 37.0909° N, longitude −2.3581° E, altitude 500 m a.m.s.l., semi-arid climate) usually takes place continuously over the course of 30 to 120 days while the test RSI is positioned within less than 10 m from the reference instruments. However, since RSIs are mostly employed in the context of CSP, only measurements under CSP operating conditions are included in the calculation of calibration factors. These conditions are specified later in detail. Due to the manifold environmental and operational influences which can occur during this time span, the raw data needs to be screened and manually reviewed for errors and temporary system failures. The calculation of the calibration factors is based on minimizing the root mean square deviation (RMSD) but differs for both methods.

Another approach to RSI calibration was published in Kern (2010) which only compares GHI measurements from the photodiode to a reference and thus replaces the sensor manufacturer's calibration factor. However, this method is not subject of this paper.

2.1 Calibration method DLR2008

This calibration method assigns two calibration factors: CFG for GHI and CFD for DHI which are applied in accordance to Eqs. (1) to (3). Since both GHI and DHI have different spectral compositions the sensor's responsivity differs among the two. The typical difference in responsivity is incorporated into the correction functions and hence the correction refers to the responsivity for the two components averaged over the group of instruments used for the development of the correction functions. However, the difference in responsivity for GHI and DHI is specific to each individual sensor as deviations of the spectral response between different instruments occur. Thus, better results are achieved by using separate calibration factors (Geuder et al., 2008). Because DNI is

AMTD
8, 10249–10282, 2015

the desired measurand, CFG is optimized for determination of the DNI. The improved version presented in Geuder et al. (2010) allows a separate adjustment of calibration constants for GHI and DNI.

The functionally corrected and calibrated GHI is obtained by multiplying the calibration factor CFG to the functionally corrected global horizontal irradiance (GHI_{cor}):

$$GHI_{RSI} = CFG \times GHI_{cor} \quad (1)$$

The calculation of the functionally corrected and calibrated DHI differentiates between two cases. While the uncorrected DNI is at $2\,W\,m^{-2}$ or above:

$$DHI_{RSI} = CFD \times DHI_{cor} \quad (2)$$

If the uncorrected DNI is lower than $2\,W\,m^{-2}$:

$$DHI_{RSI} = CFD \times GHI_{cor} \quad (3)$$

The reason is that at such low DHI values usually no DNI is prevailing and thus DHI is equal to GHI; then the GHI value measured each second is more accurate than the DHI value derived from the measurement during the brief rotation.

The corrected and calibrated DNI, DNI_{cor} is determined from the corrected and calibrated GHI_{RSI}, DHI_{RSI} and the solar zenith angle SZA.

$$DNI_{RSI} = \frac{GHI_{RSI} - DHI_{RSI}}{\cos(SZA)} \quad (4)$$

The data collection and documentation is performed as explained in the following. First, GHI_{Ref}, DHI_{Ref} and DNI_{Ref} are sampled every second and recorded as one minute average values as well as the ambient pressure and temperature. Then the RSI values for GHI, DHI and DNI are averaged and recorded once per minute. The sampling rate before calculation of one minute values differs for RSR2 (irradiance Inc.), RSP-4G (Reichert GmbH) and Twin-RSI (CSP Services GmbH) as detailed in Table 1. In RSP-4G and Twin-RSI sensors also the sensor temperature is recorded.

Discussion Paper | Discussion Paper | Discussion Paper | Discussion Paper |

AMTD

8, 10249–10282, 2015

The next step is the monitoring of the measurements. In order to identify and resolve operational problems, the recorded data of all instruments is scrutinized at least once per weekday by manually reviewing the reference and test data. Furthermore, the instruments are cleaned and inspected every weekday in situ for anomalies. The exact time of each cleaning event is documented. The redundant GHI measurement is used to control the operation of the reference instruments. Operational errors are documented in the calibration database. All relevant events concerning the measurement station and in the vicinity (e.g. construction works, maintenance of nearby instruments) are documented.

The data treatment includes the following steps. For each data channel 10 min mean values are calculated from the recorded 1 min averages: performing the calibration in 10 min time intervals reduces the signal deviation between reference and RSI at intermediate skies which results from the distance between the sensors and moving clouds. Then a screening algorithm performs a quality check of all recorded channels as recently presented in (Geuder et al., 2015). Among others, the quality check tests and marks if measured values are physically possible, if their fluctuation (or lack of it) is realistic and if the data points have been manually flagged/commented during the measuring period. Furthermore, a soiling correction algorithm is applied to DNI_{Ref} in accordance to the documented cleaning events following the method from Geuder and Quaschning (2006). Then, the LI-COR calibration factor CF_{Licor} is applied to the RSI data.

Afterwards, the not yet calibrated and still uncorrected RSI time series, reference time series and time series of the signal deviations are checked for consistency by an expert. If one of the six irradiances seems to be unreliable, it is removed from the calibration dataset.

For RSI without temperature sensor (e.g. RSR2) the sensor temperature is estimated using the following Eq. (5) from Wilbert et al. (2015) based on GHI and ambient tem-

AMTD
8, 10249–10282, 2015

perature T_{amb}:

$$T_{RSI} = T_{amb} + \left(-4.883 \times 10^{-6} \times GHI_{raw}^2 + 0.00953 \times GHI_{raw} - 0.5\right) \quad (5)$$

Another estimation algorithm substitutes missing pressure measurements in all RSIs using the barometric formula. This is used in calculation of the apparent solar angle including refraction and in particular required at low solar elevations.

Then the GHI_{Ref} is calculated by using the apparent sun height at the middle of each 10 min interval and the irradiance data are compared again. First, the deviation of GHI_{raw}, DHI_{raw} and DNI_{raw} (RSI data with applied CF_{Licor}) and the reference data are checked for plausibility by comparison against the reference irradiance components in scatterplots for each component. Implausible data are removed. Irradiance data which has been flagged by the screening algorithm is marked in the scatterplots and excluded as well as potentially erroneous. In a second check the deviation of RSI data from the reference data before and after application of the functional corrections (specific to the calibration method, here DLR2008) are compared to each other. Criteria for implausible data include high deviation between reference DNI (pyrheliometer) and calculated DNI from the reference pyranometers (> 8 % for SZA < 75°; > 15 % for greater SZAs) and high deviations between test and reference instruments (> 25 %). Erroneous data is marked for exclusion and a comment is saved in the database.

The central step is the calculation of calibration factors. The solar elevation angle, GHI_{Ref} and DHI_{Ref} as well as their deviation from the functionally corrected but not yet calibrated RSI measurements GHI_{cor} and DHI_{cor} are filtered for their respective calibration limits (Table 2). The calibration limits define the acceptable range of irradiance and solar elevation angle for calibration as specified in Table 2. Then the DHI calibration factor CFD is determined by minimization of the RMSD of DHI_{RSI} from DHI_{Ref} through variation of CFD. Thereafter, while ignoring the previous GHI and DHI data screening the solar elevation angle, DNI_{Ref} and its deviation from the corrected RSI measurement DNI_{cor} is screened for its calibration limits (Table 2). With applied CFD calibration factor the screened data is used to determine the calibration factor CFG for GHI by minimization of the RMSD of DNI_{RSI} from DNI_{Ref} by variation of CFG.

Finally, the calibration results are manually reviewed. The deviation of corrected RSI data from the reference before and after calibration is compared. Bias, standard deviation and RMSD of the corrected and calibrated RSI data from the reference are calculated and serve as indicators for the quality of the calibration. If further erroneous data is found, it can be marked for exclusion and the calculation of the calibration constants is repeated.

The calibration procedure for the improved version (Geuder et al., 2010) is similar to the described one with the exception that CFG is optimised for GHI (instead of DNI). Here, two further calibration constants for DNI are introduced and fitted to the DNI in dependence on its intensity after several filtering steps. This method however is not analysed here.

2.2 Calibration method VigKing

VigKing determines three separate calibration factors CFg, CFd and CFn for GHI, DHI and DNI respectively (Geuder et al., 2011). Each calibration factor is optimized for RMSD of the irradiance component it is applied to.

The calibration factors are applied in accordance to Eqs. (6)–(9). The functionally corrected and calibrated GHI (GHI_{RSI}) is obtained by multiplying the functionally corrected GHI_{cor} by the GHI calibration factor CFg

$$GHI_{RSI} = CFg \times GHI_{cor} \tag{6}$$

The DHI correction is given with the functionally corrected GHI_{cor} as a parameter. After calibration the functionally corrected and calibrated DHI_{RSI} is calculated along the corrections from (Vignola, 2006) with GHI_{RSI} as GHI input.

If $GHI_{RSI} \leq 865.2\,\mathrm{W\,m^{-2}}$ the DNI is calculated along Eq. (7)

$$DHI_{RSI} = CFd \times \left[DHI_{raw} + GHI_{RSI} \times \left(-9.1 \times 10^{-11} \times GHI_{RSI}^3 + 2.3978 \times 10^{-7} \times GHI_{RSI}^2\right.\right.$$

AMTD
8, 10249–10282, 2015

Calibration methods for rotating shadowband irradiometers

W. Jessen et al.

$$-2.31329234 \times 10^{-4} \times \mathrm{GHI_{RSI}} + 0.11067578794\Big)\Big] \quad (7)$$

and Eq. (8) is used, if $\mathrm{GHI_{RSI}} > 865.2\,\mathrm{W\,m^{-2}}$.

$$\mathrm{DHI_{RSI}} = \mathrm{CFd} \times \left[\mathrm{DHI_{raw}} + \mathrm{GHI_{RSI}} \times \left(0.0359 - 5.54 \times 10^{-6} \times \mathrm{GHI_{RSI}}\right)\right] \quad (8)$$

The corrected and calibrated $\mathrm{DNI_{RSI}}$ is determined with the DNI calibration factor CFn as

$$\mathrm{DNI_{RSI}} = \mathrm{CFn} \times \frac{\mathrm{GHI_{RSI}} - \mathrm{DHI_{RSI}}}{\cos(\mathrm{SZA})}. \quad (9)$$

Note that the application of three calibration factors results in not completely self-consistent combinations of DNI, GHI and DHI. The calibration factor CFn is usually between 1.005 and 0.995 and hence the self-inconsistency is not very pronounced. The average of the absolute amount of 1-CFn for 76 calibrations carried out at PSA between September 2013 and August 2015 is 0.0057.

In all aspects other than the correction functions and the assignment of a third calibration factor, the VigKing calibration method is identical to the method DLR2008 presented in Sect. 2.1. In deviation from the account given in Geuder et al. (2011) in todays practice the same calibration limits (Table 2) are used in both calibration methods. The determination of the three calibration constants is done as follows.

$\mathrm{GHI_{Ref}}$ and $\mathrm{DHI_{Ref}}$ as well as their deviation from the corrected but not yet calibrated RSI measurements $\mathrm{GHI_{cor}}$ and $\mathrm{DHI_{cor}}$ are filtered for their respective calibration limits and solar elevation angle (Table 2). The screened data is then used to determine the GHI calibration factor CFg by minimization of the RMSD of the corrected and calibrated $\mathrm{GHI_{RSI}}$ from $\mathrm{GHI_{Ref}}$. Thereafter, the previous data screening for calibration limits is repeated with applied CFg before the screened data is used to determine the DHI calibration factor CFd by minimization of the RMSD of the corrected and calibrated $\mathrm{DHI_{RSI}}$ from $\mathrm{DHI_{Ref}}$. Then, with applied CFg and CFd, the corrected but not yet calibrated RSI measurement $\mathrm{DNI_{cor}}$ is screened for calibration limits (Table 2). Finally the

AMTD
8, 10249–10282, 2015

screened data is used to determine the DNI calibration factors CFn by minimization of the RMSD of the corrected and calibrated DNI_{RSI} from DNI_{Ref}.

3 Evaluation of RSI calibration duration and seasonal influences

A first site specific assessment of the necessary calibration duration at PSA has been presented in Geuder et al. (2014) in which a minimum measuring period of 30 days was recommended based on data collected from a single instrument. We investigated the subject further by use of a total of seven long-term data sets ranging from 251 to 1289 days duration collected over a period of 6.5 years from five RSI instruments (Table 2). Calibrating an instrument with the entire available long-term measuring period is considered the best achievable result.

Based on an application of moving averages the fluctuation of calibration results for different calibration durations was compared to the result of a long-term calibration over the whole period of available data. This was done separately for each of the seven long-term data sets. The deviation of calibration results from a long-term calibration in regard to DNI is represented by Π_{DNI} as defined in the following.

First the instrument is calibrated over the entire available long-term measuring period. The thereby derived calibration factors are applied to the functionally corrected 10 min mean values of RSI measured irradiance from the calibration period. The same manual and automatic data exclusions including the calibration limits as applied during the calibration process are kept in place while calculating the ratio of reference to RSI irradiance along Eq. (10). The timestamp t indicates the 10 min interval.

$$R_{DNI}(t) = \frac{DNI_{Ref}(t)}{DNI_{RSI}(t)} \tag{10}$$

Thereafter, the moving average (here: moving in steps of 24 h) of R_{DNI} is calculated as

$$M_{R,DNI}(T, t_d) = \frac{1}{n} \times \sum_t R_{DNI}(t) \text{ with } t \in \left[t_d - \frac{T}{2}, t_d + \frac{T}{2}\right] \tag{11}$$

AMTD
8, 10249–10282, 2015

where t_d represents a timestamp at noon and T is the duration of the moving interval in days. n is the number of timestamps within each interval defined by t_d and T.

Additionally, $L_{R,DNI}$ the mean of R_{DNI} over the entire measurement series is calculated along the equation

$$L_{R,DNI} = \frac{1}{m} \times \sum_t R_{DNI}(t) \tag{12}$$

where m is the number of timestamps within the whole series. Finally, Π_{DNI} is calculated as the ratio of the moving average $M_{R,DNI}$ to the mean of R_{DNI} over the entire calibration period represented by $L_{R,DNI}$.

$$\Pi_{DNI}(T,t_d) = \frac{M_{R,DNI}(T,t_d)}{L_{R,DNI}} \tag{13}$$

The evaluation method as described above was applied separately for both calibration methods DLR2008 and VigKing and its findings are discussed in the following sections.

3.1 Evaluation results for the method DLR2008

Figure 2 displays the distribution of Π_{DNI} for each RSI data set (Table 3) and for varying calibration duration in form of boxplots. In the type of boxplots used in this paper the whiskers include 99.3 % of all values in the case of normal distribution. The box itself includes 50 % of all values with the first quartile below and the third quartile above its edges. The horizontal line signifies the median while the circle symbolizes the arithmetic mean.

As expected, the whiskers of each data set get closer to zero with increased calibration duration T since the influence of isolated extreme spectral conditions is evened out by the greater amount of data used. Similarly, the overall presence of outliers (exceptionally deviating calibration results) is reduced significantly. Due to the high volatility

AMTD
8, 10249–10282, 2015

of calibration results for measuring periods below 14 days as seen in Fig. 2 such durations are considered as insufficient. In comparison to all other sensors, increasing the calibration duration from 1 to 30 days does not decrease the interquartile ranges significantly for the RSR2-0039-1. Since the power supply of the RSR2-0039 had to be exchanged between the measurement sets RSR2-0039-1 and RSR2-0039-2, we assume that this defect is the reason for the behaviour.

Calibrations of 180 days duration or more on the other hand are too time-consuming in practice, especially in consideration of the recommended frequency of recalibration of 2 years given in Geuder et al. (2014). Another disadvantage of very long-term calibrations is the lag time. Therefore, further analysis focuses on durations of 14, 30, 60, 90 and 120 days.

The Π_{DNI} were plotted over the time span of the long-term calibration measuring for one RSI data set at a time as shown in Fig. 3 for the RSP-4G-08-10-3 data set and calibration durations of $T = 14$, $T = 60$, $T = 90$ and $T = 180$ days. The horizontal axis represents the date and the first day of each month is represented by vertical gridlines. The left vertical axis displays Π_{DNI} while the second vertical axis provides the daily number of usable timestamps. In this representation each plotted data point refers to the middle timestamp of its interval t_d.

The number of usable timestamps per day clearly coincides with the seasons. This is common to all data sets (Table 3) at hand and is a correlation to the daily daylight hours. Therefore, a calibration of the same duration differs in the amount of usable data in dependence on the time of the year.

In order to derive recommendations in regard to the necessary calibration duration for different times of the year, the Π_{DNI} of the seven data sets (Table 3) was sorted by the starting month of calibration and the combined distribution of all RSI data sets was visualized in boxplots as presented in Fig. 4. This allows choosing the required duration in dependence of the starting time of measurements and the acceptable distribution of Π_{DNI}. The same was done for Π_{GHI} and Π_{DHI} in Figs. 5 and 6. Since most of the time the greater part of GHI is due to DNI in CSP relevant regions, the seasonal course of Π_{GHI}

AMTD
8, 10249–10282, 2015

(Fig. 5) distributions displays more similarities with the seasonal course of distributions of Π_{DNI} (Fig. 4) than of Π_{DHI} (Fig. 6). The highest volatility is observed in Π_{DHI}.

Most boxes in Fig. 4 are well centered on their respective arithmetic mean. The course of the Π_{DNI} reaches its maximum between November and January and its minimum between March and May. This indicates a small seasonal dependence of the calibration results. The maximum for the longest calibration duration of 120 days is reached in October, two month before the maximum for 14 days calibration duration. This is due to the different calibration data set and the application of the starting month for the horizontal axis. The general observation is that the longer the calibration duration the closer the outcome will be to a long-term calibration. In the case that the conditions of the long-term calibration represent the application conditions, a long-term calibration has hence to be preferred. While this is true in most cases, some exceptions can be found. In Fig. 4 for starting dates in November and $T = 60$ days the Π_{DNI} are distributed further from zero than with any other of the evaluated durations T. This is true for all statistical values that the boxplot provides (whiskers, mean, ...). However, a duration of $T = 60$ days exhibits better distributions of Π_{DNI} than durations of 14 and 30 days for starting dates in the following month of December (better in terms of coincidence with $\Pi_{DNI} = 0$). For starting dates in January, the differences between the distribution of Π_{DNI} for 30 days and 60 days duration is further increased. This indicates that the meteorological conditions in November and February are generally more suitable for DLR2008 calibration and later RSI application at PSA than in December and January.

Furthermore, starting dates in January produced closer coincidence between Π_{DNI} and zero with a duration of $T = 90$ days than a duration of $T = 120$ days. The Π_{DNI} of starting dates in February exhibited the closest coincidence with zero for durations of $T = 60$ days along with $T = 30$ days. 90 days periods starting in January and 60 days periods starting in February have in common that they end in April while the respective longer periods include all of April and a part of May. Remarkably, the duration $T = 120$ days generated the greatest deviation of Π_{DNI} values from zero for starting

AMTD
8, 10249–10282, 2015

dates in February. This is owed to the inclusion of the entire period of meteorological conditions in April and May.

However, out of all data visualized in Fig. 4 the Π_{DNI} distributions for starting dates in May and June with T = 120 days exhibited the smallest distance between upper and lower whiskers as well as the closest coincidence with 0 % since the respective periods of time are dominated by the more suitable conditions from June onward.

As shown by these examples, the rough rule that longer calibration durations yield better results does not always apply, due to the meteorological conditions (i.e. spectral composition of irradiance) at the time. Exceptions have to be considered as discussed in the following.

Recommendations for choice of calibration duration

In consideration of the seasonal tendencies it is recommendable to vary the calibration duration in dependence on the month in which the measurements are commenced. This allows to keep the monthly maximum deviation of $M_{R,DNI}$ (Eq. 11) from $L_{R,DNI}$ (Eq. 12) within a given maximum (hereafter called $\Pi_{DNI.max}$) and thus creates results of closer to constant viability while minimizing calibration duration. Table 4 provides a summary of required minimum durations for varying $\Pi_{DNI.max}$. The mentioned exceptions are marked in the table and explained in the caption. For example, even if a constant calibration duration of T = 60 days is preferred to choosing the duration individually by month of the year, it should be considered to reduce the duration for calibrations starting in November to T = 30 days only, since for this month a duration of T = 60 days exhibited the highest Π_{DNI} in comparison to any other examined duration between 14 and 120 days.

The evaluation of seasonal influences was used to establish the correlation between $\Pi_{DNI.max}$, calibration duration and the month in which a calibration is commenced. Since Π_{DNI} represents the deviation of individual short-term calibrations from the result of a long-term calibration, $\Pi_{DNI.max}$ in combination with the relative standard uncertainty of the reference pyrheliometer (DNI_{Ref}) can be used for a conservative estimate of

AMTD
8, 10249–10282, 2015

Calibration methods for rotating shadowband irradiometers

W. Jessen et al.

calibration uncertainty:

$$\Delta \mathrm{DNI}_{\mathrm{cal,\ rel}} \approx \sqrt{\left(\Delta \mathrm{DNI}_{\mathrm{Ref,\ rel}}\right)^2 + \left(\Delta \mathrm{Soil}_{\mathrm{ph}}\right)^2 + \left(\Pi_{\mathrm{DNI,max}}\right)^2}. \tag{14}$$

In accordance with WMO (2010) the relative uncertainty of our reference pyrheliometer is 1.8 % (95 % confidence level). We hence assume $\Delta \mathrm{DNI}_{\mathrm{Ref,\ rel}} = 0.9\,\%$ for the standard uncertainty. Additionally, an uncertainty due to pyrheliometer soiling of $\Delta \mathrm{Soil}_{\mathrm{ph}} \approx 0.2\,\%$ can be estimated in respect of the findings in Geuder and Quaschning (2006).

An exemplary calculation for $\Pi_{\mathrm{DNI.max}} = 2.25\,\%$ results in an estimated $\Delta \mathrm{DNI}_{\mathrm{cal,\ rel}} \approx 2.4\,\%$ of the calibration uncertainty. It should be mentioned that this estimation includes the uncertainty caused by the spectral response of the solid state pyranometer that has to be expected for application at PSA after the calibration at PSA. Also other uncertainty contributions as e.g. directional, linearity and temperature effects are partly included in this estimation because the bulk of the data in a calibration periods might belong to confined ranges of these parameters.

3.2 VigKing

The duration of VigKing calibrations is evaluated in the same fashion as done in the previous section for DLR2008.

In comparison to DLR2008, the VigKing method results in similar seasonal distributions of Π_{DNI}. The rough rule that longer calibrations result in less deviations from the long-term calibration also holds in this case. However, some differences can be found. In Fig. 7 it is noticeable that the VigKing produces wider interquartile ranges of Π_{DNI}. This is especially true for starting dates during the time from November to January. During this period the distributions are exceptional symmetrically centered around zero but exhibit the widest range of Π_{DNI} values.

With calibration method VigKing (Fig. 7) the Π_{DNI} distributions for starting dates in March were the closest to zero for durations of 30 days. Contrarily, in the following two

AMTD
8, 10249–10282, 2015

months of April and May the distributions of Π_{DNI} for a duration of $T = 30$ days deviates further from zero than for other durations. This observation indicates that the meteorological conditions during April and May are not well suited for VigKing calibrations. In the case of calibrations which start in April or May but reach well into the months of June or July a far closer coincidence of the Π_{DNI} with zero is achieved. This is caused by the more suitable conditions from June onward. A similar tendency was observed in DLR2008 (Fig. 4).

In DLR2008 the duration of 60 days produced the highest upper Π_{DNI} whiskers among calibrations starting in November (Fig. 4). This is not true for VigKing (Fig. 7) where only $T = 14$ days exhibits higher values than $T = 60$ days. On the other hand, in regard to maximum Π_{DNI} and interquartile range a duration of $T = 30$ days exhibits a more desirable distribution for this starting month than a duration of 60 days.

Measurements starting in October with 30 to 90 days duration resulted in smaller Π_{DNI} than 120 days duration due to the adverse conditions during the winter months. In consideration of the interquartile ranges of Π_{DNI} a duration of 90 days appears to perform best for calibration starting in the month of October.

Recommendations for choice of calibration duration

Similarly as for DLR2008 calibrations, a table has been comprised to choose the calibration duration for VigKing in dependence on the month of the year and the desired $\Pi_{DNI.max}$ (Table 4).

If a constant calibration duration throughout the year is preferred, also for VigKing a duration of $T = 60$ days is advised as a trade-off between producing results close to a long-term calibration and not consuming more time than reasonable. Similarly to DLR2008 one should resort to a shorter duration of $T = 30$ days for calibrations starting in November. In VigKing the same is true for calibrations starting in March. Figure 7 suggests a deviation from a long-term calibration below 2 % for $T = 60$ days throughout the year.

AMTD
8, 10249–10282, 2015

4 Conclusions

The influence of the RSI calibration duration and the seasonal fluctuations of two calibration methods at PSA were investigated. Small but noticeable seasonal dependencies were observed. Also some fluctuations of RSI calibration results were found that are influenced by the calibration duration. Thus, it was possible to quantify relations which can be used to optimize the calibration duration in dependence on the time of the year in which a calibration takes place.

Additionally, the findings allowed the identification of periods with higher likelihood of adverse meteorological conditions (November to January and April to May). Consequently, the duration of data acquisition for calibrations starting during these months should generally be longer than for calibrations starting during the rest of the year. In some cases it is advantageous to limit the duration of calibrations starting before these periods so that these periods are not used.

In order to apply the results of this analysis, two tables where comprised which allow to choose the calibration duration for both calibration methods in dependence on the month of the year in which measurements are commenced and the maximum tolerable value of $\Pi_{\text{DNI.max}}$ which represents the fluctuation of calibration results (Tables 4 and 5). For DLR2008 a constant calibration duration of 30 days throughout the year with the exception of calibrations starting in December (60 days) is sufficient to keep $\Pi_{\text{DNI.max}}$ within 2.5 %. In VigKing calibrations the same applies with the exception of using 60 days duration for calibrations starting in the month of May instead of December.

To make a final statement on the subject of calibration uncertainty is not within the scope of this work. This is the subject of further investigation. Based on the observation that during certain times the deviation of calibration results exhibits one-sided tendencies towards the positive (November to January) or the negative (April and May) it could be investigated, if during RSI calibration these seasonal effects can be compensated by additional or improved functional corrections. Further investigation may also

AMTD
8, 10249–10282, 2015

include the application of the presented evaluation methods to the improved version of DLR2008.

Acknowledgements. The RSR2 data sets were courteously provided by Suntrace GmbH for which the authors wish to express their gratitude. DLR also thanks the EU for partially funding this research activity within the FP7 project SFERA2.

The article processing charges for this open-access publication were covered by a Research Centre of the Helmholtz Association.

References

Augustyn, J., Geer, T., Stoffel, T., Kessler, R., Kern, E., Little, R., Vignola, F., and Boyson, B.: Update of algorithm to correct direct normal irradiance measurements made with a rotating shadowband pyranometer, in: Proc. Solar 2004, American Sollar Energy Society, Portland, OR, 2004.

Geuder, N. and Quaschning, V.: Soiling of irradiation sensors and method for soiling correction, Sol. Energy, 80, 1402–1409, 2006.

Geuder, N., Pulvermüller, B., and Vorbrugg, O.: Corrections for rotating shadowband pyranometers for solar resource assesment, in: Solar Energy + Applications, Proceedings of SPIE (The International Society for Optical Engineering), 70460F, doi:10.1117/12.797472, 2008.

Geuder, N., Affolter, R., Goebel, O., Dahleh, B, Al Khawaja, M., Wilbert, S., Pape, B., and Pulvermueller, B.: Validation of direct beam irradiance measurements from rotating shadowband pyranometers in a different climate, in: SolarPACES 2010, 21–24 September 2010, Perpignan, France, Journal of Solar Energy Engineering, accepted, 2010.

Geuder, N., Hanussek, M., Haller, J., Affolter, R., and Wilbert, S.: Comparison of corrections and calibration procedures for rotating shadowband irradiance sensors, in: SolarPACES 2011, 20–23 September 2011, Granada, Spain, 2011.

Geuder, N., Affolter, R., Kraas, B., and Wilbert, S.: Long-term Behavior, Accuracy and Drift of LI-200 Pyranometers as Radiation Sensors in Rotating Shadowband Irradiometers (RSI), in: SolarPACES 2013, 17–20 September 2013, Las Vegas, USA, Energy Procedia no. 49, 2330–2339, doi:10.1016/j.egypro.2014.03.247, 2014.

AMTD

8, 10249–10282, 2015

Calibration methods for rotating shadowband irradiometers

W. Jessen et al.

Geuder, N., Wolfertstetter, F., Wilbert, S., Schüler, D., Affolter, R., Kraas, B., Lüpfert, E., and Espinar, B.: Screening and Flagging of Solar Irradiation and Ancillary Meteorological Data, Energy Procedia no. 69, 1989–1998, doi:10.1016/j.egypro.2015.03.205, 2015.

Harrison, L., Michalsky, J., and Berndt, J.: Automated multifilter rotating shadow-band radiometer: an instrument for optical depth and radiation measurements, Appl. Optics, 33, 5118–5125, 1994.

ISO 9059: Solar Energy – Calibration of Field Pyrheliometers by Comparison to a Reference Pyrheliometer, International Organization for Standardization, Geneva, Switzerland, 1990.

ISO 9060: Solar Energy – Specification and Classification of Instruments for Measuring Hemispherical Solar and Direct Solar Irradiation, International Organization for Standardization, Geneva, Switzerland, 1990.

ISO 9847: Solar Energy – Calibration of Field Pyranometers by Comparison to a Reference Pyranometer, International Organization for Standardization, Geneva, Switzerland, 1992.

ISO 9846: Solar Energy – Calibration of a Pyranometer Using a Pyrheliometer, International Organization for Standardization, Geneva, Switzerland, 1993.

Kern, E: Calibration methods for silicon photodiode pyranometers used in rotating shadowband radiometers, in: SolarPACES 2010, 21–24 September 2010, Perpignan, France, 2010.

King, D. L. and Myers, D. R.: Silicon-photodiode pyranometers: Operational characteristics, historical experiences, and new calibration procedures, Photovoltaic Specialists Conference, 29 September 1997–03 October 1997, Anaheim, CA, 1285–1288, doi:10.1109/PVSC.1997.654323, 1997.

King, D. L., Boyson, W. E., Hansen, B. R., and Bower, W. I.: Improved accuracy for low-cost solar irradiance sensors, in: 2nd World Conference and Exhibition on Photovoltaic Solar Energy Conversion Proceedings, 6–10 July 1998, Vienna, Austria, 1998.

LI-COR: Radiation Measurement Instruments, Technical report, LI-COR Biosciences, Lincoln, Nebraska, USA, 2004.

Maxwell, E. L., Wilcox, S. M., Cornwall, C., Marion, B., Alawaji, S. H., bin Mahfoodh, M., and Al-Amoudi, A.: Progress Report for Annex II–Assessment of Solar Radiation Resources in Saudi Arabia 1993–1997, NREL/TP-560-25374, National Renewable Energy Lab., Golden, Colorado, USA, 1999.

Pape, B., Batlles, J., Geuder, N., Zurita Piñero, R., Adan, F., and Pulvermüller, B.: Soiling Impact and Correction Formulas in Solar Measurements for CSP Projects, SolarPaces, Berlin, Germany, 2009.

Vignola, F.: Removing systematic errors from rotating shadowband pyranometer data, in: Solar 2006, American Solar Energy Society, 7–13 July 2006, Denver, Colorado, USA, 2006.
Wilbert, S., Geuder, N., Schwandt, M., Kraas, B., Jessen, W., Meyer, R., and Nouri, B.: Best practices for solar irradiance measurements with rotating shadowband irradiometers, in: Technical Report IEA Task 46, Subtask B1 and INS project 1268, IEA SHC, 2015.
WMO: Guide to Meteorological Instruments and Methods of Observation, WMO-No. 8, 2010 Update, (7th edn.), World Meteorological Organization, Geneva, Switzerland, 2010.

AMTD
8, 10249–10282, 2015

Calibration methods for rotating shadowband irradiometers

W. Jessen et al.

Table 1. RSR2, RSP4G and Twin-RSI sampling rates (Wilbert et al., 2015).

	Rotation frequency	GHI	DHI	DNI
Twin RSI	1 / (30 s) alternating for both sensors	1 / s	Shadowband correction averaged with previous value	Calculated from GHI, DHI and solar position as 1 min average with correction for DHI drift
RSR2	at least 1 / (30 s) up to 1 / (5 s) if 20 W m^{-2} change in GHI	1 / (5 s)	Averaged for each rotation	Averaged for each rotation
RSP4G	1 / (60 s)	1 / s	Calculated once per minute as average of two rotations	Calculated every second from 1 s GHI samples. Averaged every 60 s

Discussion Paper | Discussion Paper | Discussion Paper | Discussion Paper |

AMTD

8, 10249–10282, 2015

Table 2. Calibration limits (Geuder et al., 2011).

Reference DNI [$\mathrm{W\,m^{-2}}$]	> 300
Reference GHI [$\mathrm{W\,m^{-2}}$]	> 10
Reference DHI [$\mathrm{W\,m^{-2}}$]	> 10
Solar elevation angle [°]	> 5
Max deviation of corrected RSI from reference [%]	±25

AMTD
8, 10249–10282, 2015

Table 3. Evaluated data sets.

Instrument	From	To	Duration [days]
RSP-4G-08-10-1	08 Aug 2008	16 Sep 2009	404
RSP-4G-08-10-3	29 Jul 2010	07 Feb 2014	1289
RSR2-0017	09 Sep 2009	16 May 2010	251
RSR2-0018	17 May 2007	15 Oct 2008	517
RSR2-0036	12 Nov 2007	12 Aug 2008	274
RSR2-0039-1	12 Nov 2007	13 Aug 2008	292
RSR2-0039-2	01 Jan 2011	18 Jan 2012	382

AMTD
8, 10249–10282, 2015

Table 4. DLR2008: minimum required calibration duration in days for given maximum of Π_{DNI} and starting time.

$\Pi_{DNI,max}$	Month											
	Jan	Feb	Mar	Apr	May	Jun	Jul	Aug	Sep	Oct	Nov	Dec
±2.5 %	30	14	14	14	14	14	14	14	14	14	14	60
±2.25 %	30	14	14	14	14	14	14	14	14	14	14[1]	60
±2 %	60	14	14	14	30	14	14	14	14	14	90	90
±1.5 %	60	14	14	90	60	30	30	30	14	30	120	120
±1 %	90	30[2]	120	90	60	30	60	30	90	90	–	120
±0.75 %	90	–	–	120	90	90	90	120	–	90	–	–
lowest	90	30	120	120	120	120	120	120	120	120	120	120

[1] 60 days is not suitable.
[2] Only 60 and 30 days are suitable.

AMTD
8, 10249–10282, 2015

Table 5. VigKing: minimum required calibration duration in days for given maximum of Π_{DNI} and starting time.

$\Pi_{DNI,max}$	Month											
	Jan	Feb	Mar	Apr	May	Jun	Jul	Aug	Sep	Oct	Nov	Dec
±2.25 %	30	14	14	14	60	14	14	14	14	14	30	30
±2 %	30	14	14	60	60	14	14	14	14	14	30	30
±1.5 %	60	30	14	90	60	14	60	60	30	14	120	90
±1 %	90	60[1]	30[1]	120	90	60	120	120	90	–	–	120
±0.75 %	90[1]	–	–	120	90	60	–	–	120	–	–	–
lowest	90	60	30	120	120	90[2]	120	120	120	90	120	120

[1] Only this duration.
[2] Positioning of the interquartile range better than 120 days.

AMTD
8, 10249–10282, 2015

Calibration methods for rotating shadowband irradiometers

W. Jessen et al.

Figure 1. Rotating Shadowband Irradiometers. Left: RSR2 (irradiance Inc.), center: RSP4G (Reichert GmbH), right: Twin-RSI (CSP Services GmbH) (Wilbert et al., 2015).

AMTD
8, 10249–10282, 2015

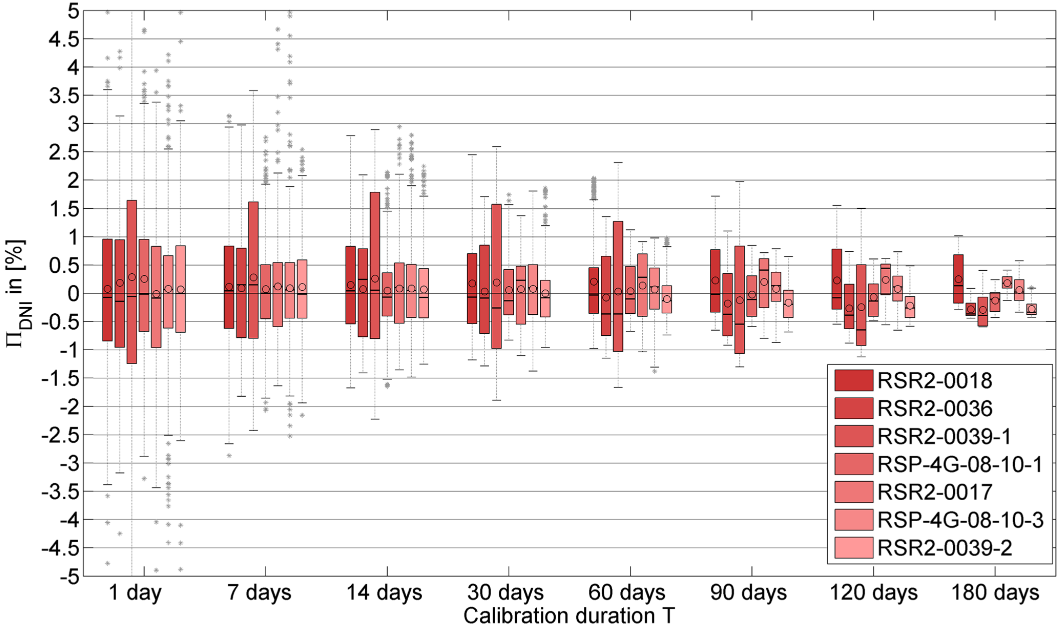

Figure 2. DLR2008: distribution of Π_{DNI} in dependence on calibration duration for seven data sets. Π_{DNI} represents the deviation of calibration results from a long-term calibration in regard to DNI.

AMTD
8, 10249–10282, 2015

Calibration methods for rotating shadowband irradiometers

W. Jessen et al.

Title Page
Abstract | Introduction
Conclusions | References
Tables | Figures
◀| |▶
◀ ▶
Back | Close
Full Screen / Esc
Printer-friendly Version
Interactive Discussion

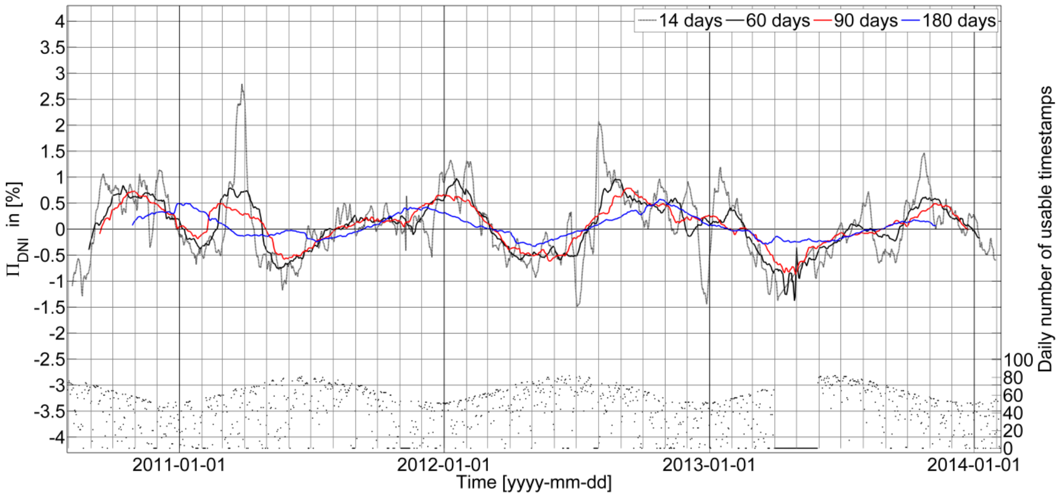

Figure 3. DLR2008: course of Π_{DNI} for varying calibration duration for RSP-4G-08-10-3 with daily number of usable timestamps. Π_{DNI} represents the deviation of calibration results from a long-term calibration in regard to DNI.

AMTD
8, 10249–10282, 2015

Calibration methods for rotating shadowband irradiometers

W. Jessen et al.

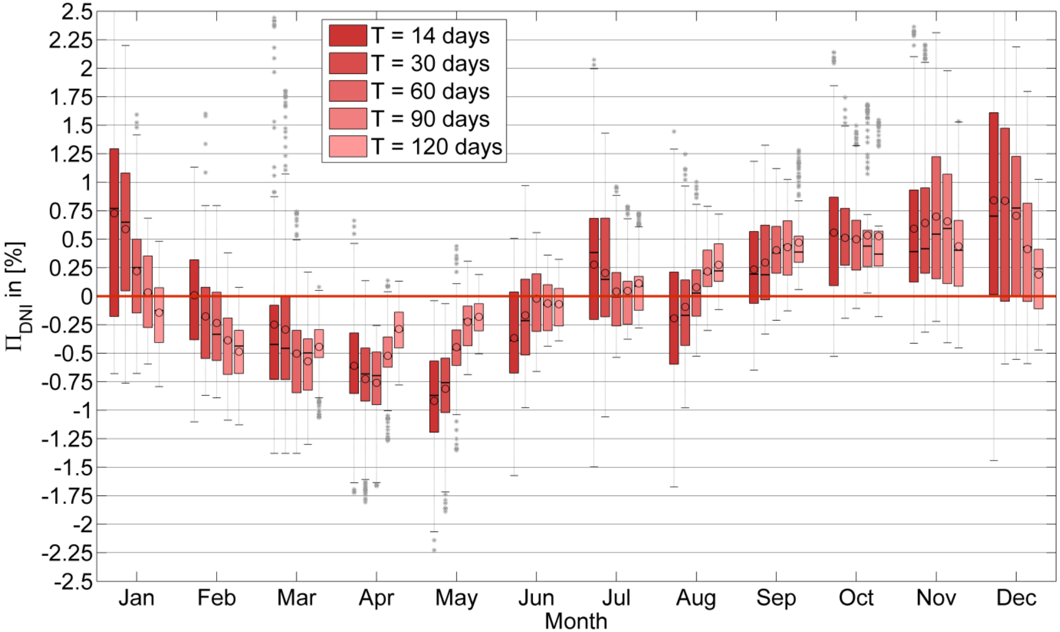

Figure 4. DLR2008: distribution of Π_{DNI} for T = 14, 30, 60, 90 and 120 days sorted by calibration starting month. Π_{DNI} represents the deviation of calibration results from a long-term calibration in regard to DNI.

AMTD
8, 10249–10282, 2015

Calibration methods for rotating shadowband irradiometers

W. Jessen et al.

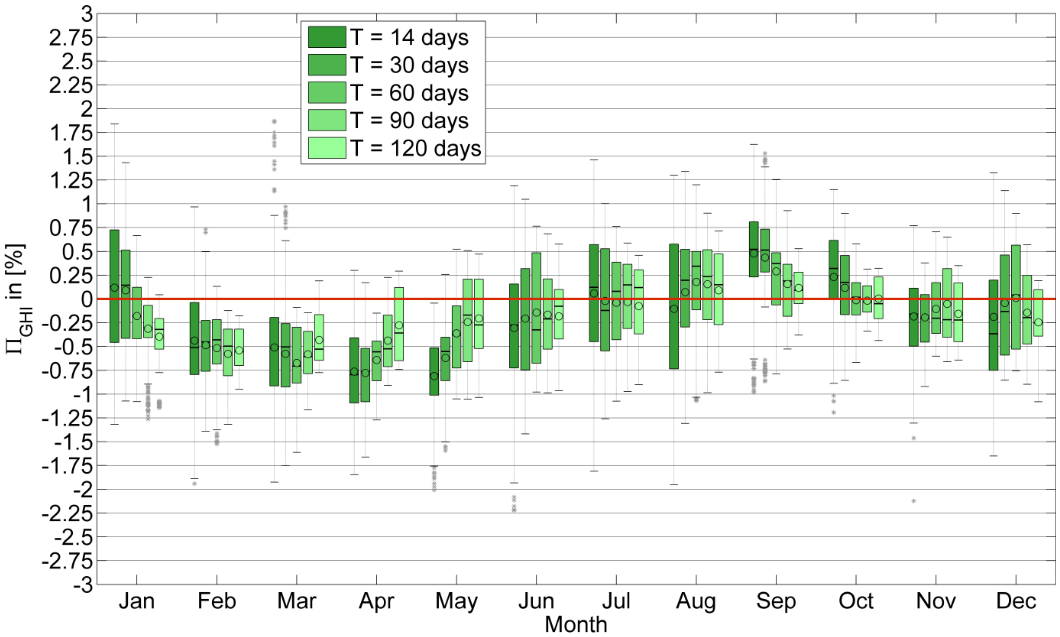

Figure 5. DLR2008: Distribution of Π_{GHI} for T = 14, 30, 60, 90 and 120 days sorted by calibration starting month. Π_{GHI} represents the deviation of calibration results from a long-term calibration in regard to GHI.

AMTD
8, 10249–10282, 2015

Calibration methods for rotating shadowband irradiometers

W. Jessen et al.

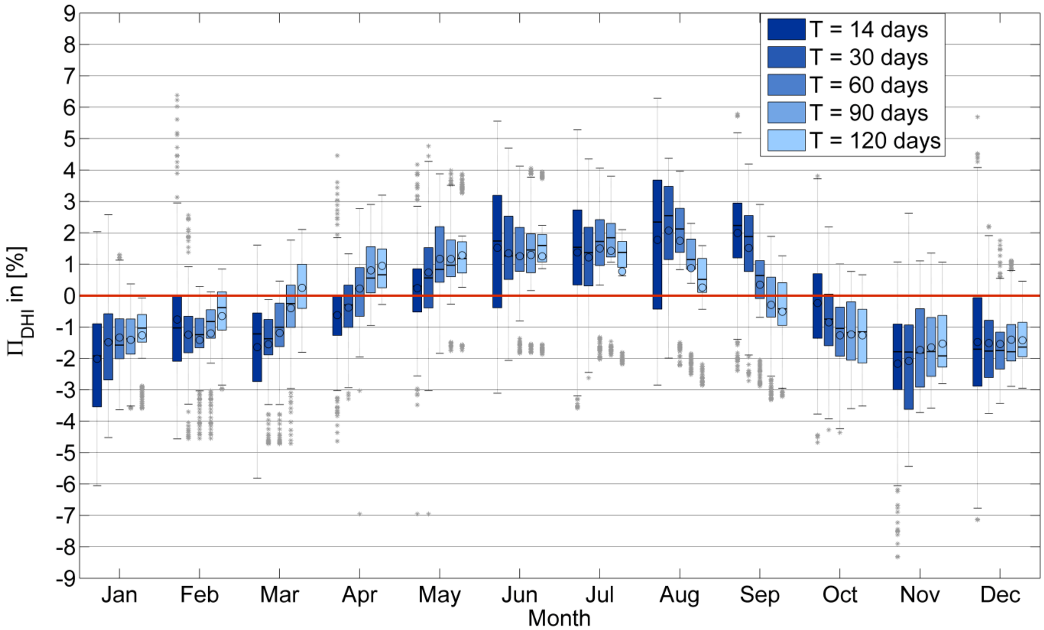

Figure 6. DLR2008: distribution of Π_{DHI} for T = 14, 30, 60, 90 and 120 days sorted by calibration starting month. Π_{DHI} represents the deviation of calibration results from a long-term calibration in regard to DHI.

AMTD
8, 10249–10282, 2015

Calibration methods for rotating shadowband irradiometers

W. Jessen et al.

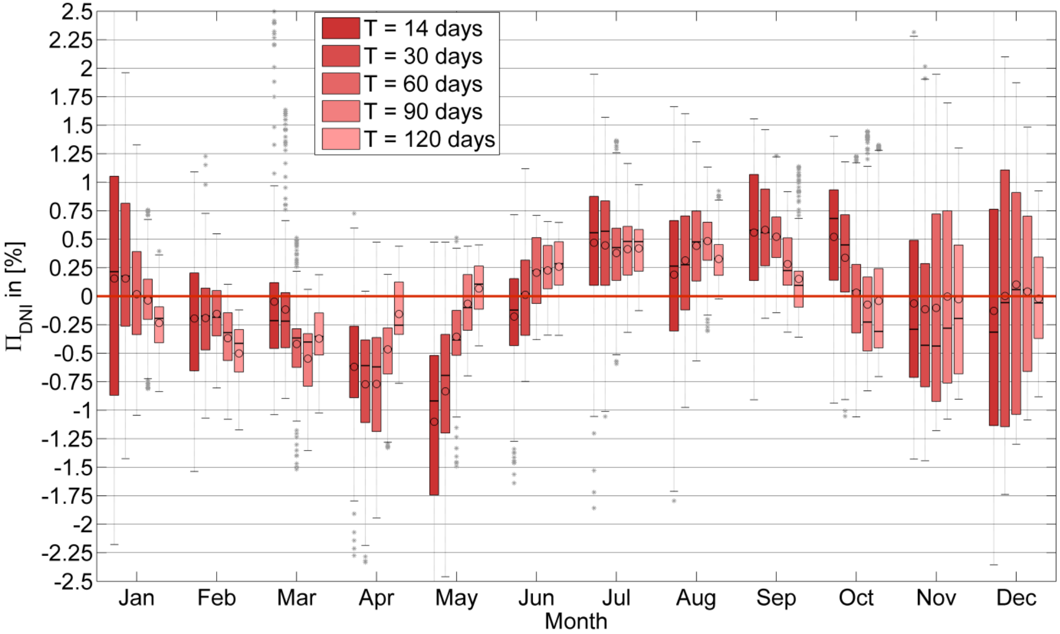

Figure 7. VigKing: distribution of Π_{DNI} for T = 14, 30, 60, 90 and 120 days sorted by calibration starting month for VigKing. Π_{DNI} represents the deviation of calibration results from a long-term calibration in regard to DNI.

AMTD

8, 10249–10282, 2015

Calibration methods for rotating shadowband irradiometers

W. Jessen et al.